

# On the Photometric Consequences of Charge-Transfer Inefficiency in WFPC2

Peter B. Stetson<sup>1, 2</sup>

Dominion Astrophysical Observatory, Herzberg Institute of Astrophysics, National  
Research Council, 5071 West Saanich Road, Victoria, British Columbia V8X 4M6, Canada

Electronic mail: peter.stetson@hia.nrc.ca

and

Mount Stromlo and Siding Spring Observatories, Institute of Advanced Studies, Australian  
National University, Weston Creek, ACT 2611, Australia

Received \_\_\_\_\_; accepted \_\_\_\_\_

---

<sup>1</sup>Guest user, Canadian Astronomy Data Centre, which is operated for the National Research Council and the Canadian Space Agency by the Dominion Astrophysical Observatory, part of the Herzberg Institute of Astrophysics

<sup>2</sup>Guest user, Isaac Newton Group Archive, which until 1998 October 31 was operated by the Royal Greenwich Observatory

## ABSTRACT

Charge-transfer effects in photometry with Wide Field Planetary Camera 2 aboard the *Hubble Space Telescope* are investigated by a comparison of WFPC2 observations with groundbased photometry for the Galactic globular clusters  $\omega$  Centauri and NGC 2419. Simple numerical formulae describing the fraction of lost signal as functions of position on the detector, stellar brightness, and the diffuse sky brightness recorded in an image are presented, and the resulting corrections are compared to those previously derived by Whitmore & Heyer (1997, *Instrument Science Report WFPC2 97-08*). Significant lost-charge effects are seen that are proportional to both the  $Y$  coordinate (*i.e.*, the number of shifts along the parallel register during readout) and the  $X$  coordinate (number of shifts along the serial register). A “typical” star image (one containing  $\sim 10^4$  photoelectrons) near the center of a “typical” intermediate-length exposure (one with a diffuse sky brightness of  $\sim 10\text{ e}^-/\text{pixel}$ , obtained at a camera temperature of  $-88^\circ\text{C}$ ) loses approximately 2% of its electrons to charge traps during readout; a star in the corner of the image most remote from the readout electronics loses twice that. The percentage of charge lost decreases as the star brightness or the diffuse sky brightness increases. Charge losses during the brief period when WFPC2 was operated at a temperature of  $-76^\circ\text{C}$  were approximately 85% greater, but apart from that no significant change in the charge transfer losses with time during the first 3.5 years of WFPC2’s mission is evident, except possibly a weak effect for the very faintest star images. These results are quite similar to those of Whitmore & Heyer, which were based on a much smaller data set, but there are some differences in detail. Even with the present set of corrections, additional sources of calibration uncertainty which I am unable to identify or characterize with the available data probably limit the

*external* accuracy of photometry from WFPC2 to of order 1–2%.

*Subject headings:* techniques: photometric

## 1. Background

The CCDs used in the Wide Field Planetary Camera 2 (“WFPC2”) of the *Hubble Space Telescope* are known to have imperfect charge-transfer efficiency (“CTE”). This property of the camera has adverse photometric consequences that have proven difficult to characterize quantitatively. The source of the problem appears to be chemical impurities in the crystal lattice of the detectors that trap some photoelectrons during exposure and readout, resulting in an underestimate of the original luminous flux impinging on the camera. These missing electrons eventually diffuse out of the traps and contribute to the background noise of that same exposure or a subsequent one. Since the charge packets that represent stellar images recorded at high row numbers must be clocked across a large fraction of the chip during readout, it is to be expected that they will encounter more traps and will lose more electrons than images recorded at lower row numbers. On the other hand, in frames where the diffuse sky brightness is high — such as in long exposures through broad-band filters — charge traps over the entire detector area can be filled by sky-generated photoelectrons. Under these circumstances, the net effect of the charge-transfer inefficiency would be a small overall lowering of the diffuse sky brightness perceived in the astronomical scene, while the apparent projection of the stellar images *above* the diffuse sky surface brightness could be comparatively unaffected. An early analysis suggested that in images where the sky brightness is low ( $\lesssim 20\text{--}30\text{ e}^-/\text{pixel}$ ) a simple “ramp” correction proportional to the  $Y$ -coordinate position of the star image, amounting to 4% per 800 rows, would approximately correct recorded fluxes for the lost electrons; in images where the sky was bright ( $\gtrsim 250\text{ e}^-/\text{pixel}$ ), no correction was needed; and in cases of moderate sky brightness an intermediate correction was recommended (Holtzman *et al.* 1995a).

While Holtzman’s ramp model corrects for the first-order effects of charge loss during readout, second-order effects may be significant. For instance, one would expect any given

charge trap to absorb only a limited number of electrons before their mutual repulsion effectively blocked the ingestion of any additional charge. Thus, faint star images consisting of comparatively few photoelectrons should lose a larger fraction of their total charge than images of bright stars containing many photoelectrons. One would therefore expect faint stars to require a larger fractional correction than bright stars near the same row number and in the presence of the same sky brightness. On the other hand, the large electron swarm corresponding to the image of a bright star would occupy a somewhat larger volume within the three-dimensional body of the detector, and might therefore actually encounter more lattice imperfections than would be accessible to smaller electron clouds. Consequently, while we might still expect that brighter stars will require smaller magnitude corrections than fainter ones, it may be that the correction will approach zero more slowly than the expected simple exponential dependence as arbitrarily bright stars are considered. In addition, while it has been demonstrated that a given star’s electron swarm can lose some charge while being clocked through some number of rows along a CCD’s parallel register, it is also possible that said packet may lose yet more charge while being transferred through some number of columns along the serial register. Again, this second ramp correction, presumably proportional to the star’s  $X$ -coordinate position in the digital image, may also depend upon the sky brightness in the scene and on the brightness of the star image itself. The numerical coefficients of the  $Y$  and  $X$  ramp corrections may be different, due to the dissimilar morphologies of the parallel and serial registers within the semiconductor material.

Whitmore & Heyer (1997; WH97) have estimated the above first- and second-order effects of the charge-transfer inefficiency in WFPC2, based upon a special sequence of observations of the globular cluster  $\omega$  Centauri (= NGC 5139). Observations were obtained at four pointings of the telescope, with deliberate translations imposed so that a particular piece of the star field could be recorded on the four different chips during the course of

the sequence. Since the natural coordinate systems of the four detectors are rotated by  $90^\circ$  with respect to each other, this allowed several hundred star images to be used for a purely differential determination of the fraction of charge lost as a function of position on the detector, without a need to know the absolute brightness of any given object. WH97 presented their results in four alternative formulations, of which the most relevant to the present discussion is given by their Eqs. 1, 2d, and 3d:

$$CTS_{\text{corrected}} = \left[ 1 + \frac{Y\text{-CTE}}{100} \times \frac{Y}{800} + \frac{X\text{-CTE}}{100} \times \frac{X}{800} \right] CTS_{\text{observed}}$$

$$Y\text{-CTE} = 10^{(0.6930 - 0.2675 \times \log BKG_{\text{blank}})}$$

$$X\text{-CTE} = 7.040 - 1.63 \times \log CTS_{\text{observed}}$$

Here,  $CTS$  represents total WFPC2 data numbers belonging to the stellar image within an aperture  $0''.5$  in radius, as perceived with the gain =  $7 \text{ e}^-/\text{DN}$  electronics;  $X$  and  $Y$  represent the position of the stellar image in the natural coordinate system of the detector (pixel (1,1) being the first one to be read through the amplifier and (800,800) being the last, with the  $X$  coordinate varying more rapidly); and  $BKG_{\text{blank}}$  is the perceived diffuse sky brightness in the scene, exclusive of recognized stellar images. (I have opportunistically adopted this version from the four variants presented, because — following Holtzman *et al.* (1995b) — in reducing WFPC2 data I routinely correct measured magnitudes to their half-arcsecond-aperture equivalents, and because the data files produced by my software contain an estimate of the local sky brightness around and underlying each detected object.)

Certain properties of these formulae may be noted.

(1) The correction that is proportional to the  $Y$  position of the star depends only on the diffuse sky brightness in the image, and not on the brightness of the star itself. In contrast, the alternative  $Y$  ramp corrections presented for magnitudes as measured through  $0''.2$  synthetic apertures depend upon both sky and star brightness. This change

in formulation stems from the finding by WH97 that the difference between magnitudes measured in 0".2 and 0".5 apertures itself depends upon the stellar brightness: “We find the CTE loss is slightly reduced when the larger aperture is used, by about 1% for the bright stars and 3% for the faint stars.” Apparently, in the data studied by WH97 this effect tended to erase the magnitude dependence of the ramp corrections in the larger aperture. However, it should be noted that a simple differencing of the formulae provided by WH97 indicates that perfect cancellation can occur only at a particular value of the sky brightness, and will not be the case in general.

(2) The correction that is proportional to the  $X$  coordinate depends only on the brightness of the star and not at all on the diffuse brightness of the sky, a result not necessarily to be predicted from the electron-trap model of the charge-transfer inefficiency.

(3) The  $Y$ -coordinate ramp is proportional to an exponential function of the logarithm of the sky brightness, so (a) the correction tends asymptotically (but slowly) to zero as the sky brightness increases without limit, but (b) as the sky brightness decreases to zero, the correction

$$10^{0.6930} \times 10^{-0.2675 \times \log BKG_{\text{blank}}} = \text{constant} \times \frac{1}{BKG_{\text{blank}}^{0.2675}} \rightarrow \infty.$$

This implies a non-physical result for a star of any apparent magnitude detected in the presence of a very low diffuse sky brightness.

(4) The  $X$ -coordinate ramp is a linear function of the logarithm of the star counts, so (a) the correction again diverges as the number of star counts approaches zero. However, in this case the divergence is not a serious drawback, since photometry of any stellar image containing that few photoelectrons is unlikely to be of genuine astronomical interest. Conversely, (b) the correction is identically zero when  $\log CTS_{\text{observed}} = 7.040/1.63 = 4.32$ , and changes sign (*i.e.*, the lattice imperfections in the serial register appear to act as electron sources rather than electron sinks) for stellar images containing more than

21,000 DN within a half-arcsecond aperture. This is approximately the amount of flux contained within a star image whose central pixel just equals the digital saturation level of the analog-to-digital converters in WFPC2 when the gain =  $7\text{ e}^-/\text{DN}$  electronics are used. Therefore, this extrapolation, too, is probably of minimal practical relevance except possibly for very bright stars observed with the high-gain electronics bay. These extrapolations do emphasize, however, that the WH97 corrections are purely empirical constructs, and are not tied directly to a self-consistent physical model of the nature of the charge-transfer inefficiency.

(5) The model correction makes no allowance for the possibility of a charge loss that is independent of position, regardless of whatever dependence it may have on either stellar brightness or sky flux. This feature of the model is a direct consequence of the experimental design, where apparent flux ratios were observed for individual stars recorded at various positions on the chips, without any consideration of (a) flux ratios for different stars with externally known magnitude differences, or (b) flux ratios for images of individual stars as recorded in frames with different exposure times. Charge losses that are independent of position may be expected within the lattice-flaw model: simply by virtue of being formed in the body of the silicon wafer in the first place, the stellar image may lose some charge to traps located near the place of its formation. In addition, any inefficiency inherent in the transfer of charge packets from the top of a parallel register to the serial register, or from the end of the serial register into the on-chip amplifier, would be perceived as a charge loss that is independent of the original location of the stellar image on the detector.

A hint that position-independent charge losses *might* be significant came from preliminary analyses of WFPC2 images of the globular clusters NGC 2419 and Palomar 4 (see W. E. Harris *et al.* 1997; Stetson *et al.* 1998, 1999). A comparison of short-exposure ( $\leq 60$  s) images to ground-based photometry of the same objects implied photometric



zero-points consistent with those found by Holtzman *et al.* (1995b) from similarly short exposures of the  $\omega$  Cen standard field. In contrast, comparison of longer ( $\geq 1200$  s) exposures of the same fields to the same ground-based photometry implied zero points that were different by approximately 0.05 mag, in the sense that the effective quantum efficiency of the detectors was higher in the longer exposures. A subsequent recalibration of the ground-based photometry, including the addition of many more independent ground-based and HST observations of NGC 2419, suggested that the original estimate of 0.05 mag might in fact have been high; the additional data suggested that an anomaly of order 0.03 mag on average might be more nearly correct. With the publication of the WH97 corrections, it is apparent that the perceived short-minus-long zero-point difference might just be a reflection of the dependence of the fractional charge loss on the total number of recorded stellar photoelectrons and on the perceived surface flux of the sky. However, it remains possible that some residual position-independent charge loss could occur.

In this paper I reinvestigate the photometric consequences of the charge-transfer inefficiency in WFPC2, based on extensive series of observations of the Galactic globular clusters  $\omega$  Centauri and NGC 2419. In addition to testing the validity of the corrections proposed by WH97 on a much larger data set, I investigate certain aspects of the problem not considered by them.

## 2. A New Analysis of Charge Loss Effects — Overview

The data analyzed in this paper are all in the public domain, and were acquired from the *HST* Science Archive of the Canadian Astronomy Data Centre. The observations include 318 individual WFPC2 exposures lying within 2 arcminutes of the nominal center of the *HST* standard calibration field in the nearby Galactic globular  $\omega$  Centauri (Equinox 2000.0 coordinates  $13^{\text{h}}25^{\text{m}}37^{\text{s}}.0$ ,  $-47^{\circ}35'38''$  according to H. C. Harris *et al.* 1993). To

these are added 91 exposures mostly centered within a few dozen arcseconds of  $7^{\text{h}}38^{\text{m}}06^{\text{s}}.8$ ,  $+38^{\circ}51'55''$ : about  $1'$  south of, but including, the center of the far-halo globular cluster NGC 2419. These latter data include all of the observations discussed by W. E. Harris *et al.* (1997), plus some additional exposures of the cluster that were obtained by STScI staff specifically to assist in the calibration of WFPC2. Some differences between the present data set and that of Whitmore & Heyer (1997) deserve particular mention.

(1) The WH97 analysis relied on eight observations made in each of the standard broad-band filters (F336W, F439W, F555W, F675W, and F814W), as well as four observations in F606W intended to allow a comparison with a skyflat developed during the Medium Deep Survey project. From each of the 44 exposures, data from only one of the four WFPC2 chips were considered in their analysis. The present study concentrates on observations made in the F555W and F814W filters ( $\omega$  Cen: 152 and 159 exposures, respectively; NGC 2419: 27 and 58 exposures), because these are particularly relevant for the *HST Key Project on the Extragalactic Distance Scale*<sup>3</sup> and for studies of certain Local Group star clusters and galaxies in which I am especially interested. Data from all four chips of each of the 402 *V* and *I* exposures were considered in the analysis below. Seven observations of  $\omega$  Cen in the intermediate-band F547M filter were also included in the reductions, to allow the eventual estimation of the fundamental photometric zero-points for this filter for a particular project, but these data were not utilized in the analysis of the charge-transfer inefficiency to be presented below.

(2) The WH97 data were all taken on 1996 June 29, whereas the  $\omega$  Cen data employed here were taken from 1994 January 11 through 1997 June 26. The NGC 2419 data were all obtained during either 1994 May 21–22 (the 28 W. E. Harris observations), 1996 December 21 (6 exposures), or 1997 November 18–19 (57 exposures). Since the

---

<sup>3</sup><http://www.ipac.caltech.edu/H0kp/>

observation date determines the spacecraft roll angle required to direct the solar panels toward the Sun while the telescope is pointed at a particular spot on the celestial sphere, the WH97 observations were all obtained at the same telescope orientation. The  $\omega$  Cen observations discussed here, having been obtained at essentially all times of the year, represent several full cycles of spacecraft roll angle. The NGC 2419 observations were also taken at several different orientations.

(3) The WH97 data were all taken with WFPC2 operating at a camera temperature of  $-88^\circ$  C, whereas 116 of the 318  $\omega$  Cen observations considered here were made at the warmer temperature of  $-76^\circ$  C used early in WFPC2’s mission; the remaining 202  $\omega$  Cen observations and all 91 NGC 2419 exposures were taken at  $-88^\circ$  C.

(4) The WH97 data were obtained with Electronics Bay 4, which gives a nominal gain of  $7\text{ e}^-/\text{DN}$ , whereas 264 of the  $\omega$  Cen observations analysed here were obtained through Electronics Bay 3 (gain approximately  $14\text{ e}^-/\text{DN}$ ). The rest of the  $\omega$  Cen and all the NGC 2419 observations were taken at  $7\text{ e}^-/\text{DN}$ .

(5) The WH97 analysis was purely differential on a star-by-star basis, considering only the flux *ratio* between two observations of a given star as a function of the positional difference between the two stellar images in the natural coordinate systems of the detectors. The new analysis will assume that the true standard-system  $V$  (Johnson) and  $I$  (Kron-Cousins) magnitudes are known *a priori* from ground-based observations of the two target fields. The transformation equations relating the *HST* natural-system magnitudes to the groundbased standard system will be determined by a robust least-squares technique, assuming that the color transformation coefficients of Holtzman *et al.* (1995b; their Table 7) are correct. The statistical solution of these equations will yield the fundamental zero points of the four WFPC2 CCDs, and the residuals of individual stars from these solutions will serve as diagnostics of the charge-transfer inefficiency.

(6) WH97 estimated the mean clear-sky surface brightness for a given frame from a star-free region near the center of the field; this value was then considered appropriate for every star in the image. The software used in the present analysis estimates a unique local sky-brightness value for every star, from the mode of brightness values in a surrounding annulus if it is aperture photometry that is being derived, or from the median brightness value at and around the position of the star in a residual image from which all known stars have been subtracted in the profile-fitting analysis. Because these individual, local brightness measurements are conveniently available, they will be used in the following analyses rather than a global average sky for the frame as a whole. For the globular-cluster images used here, there is little net difference between the two methods (typically  $\sim 0.04\text{ e}^-/\text{pixel}$ ).

Both the present study and that of WH97 include a few observations obtained with internal preflashes, whose purpose was to increase the leverage for determining the dependence of the charge loss on diffuse sky brightness: WH97 had three exposures in the F555W filter with some preflash, while the present sample includes those three plus another nine preflashed exposures of NGC 2419. In each case, the preflash produced a diffuse surface brightness averaging approximately  $175\text{ e}^-/\text{pixel}$ . In the long exposures of NGC 2419 the sky brightness was typically of order  $250\text{ e}^-/\text{pixel}$ , and in all other cases the background level was quite close to zero.

All WFPC2 images studied here were recalibrated by the Canadian Astronomy Data Centre, using the best bias and flat-field frames available at the time the data were requested. The intensities in the frames were corrected for geometric distortion, known defective pixels were masked, and the resulting images were multiplied by 4.0 and converted to short integers as described by Stetson *et al.* (1998). Instrumental magnitudes were determined via the profile-fitting technique with the computer program ALLFRAME

(Stetson 1994), and selected bright, isolated stars were used to compute magnitude corrections to a system defined by half-arcsecond synthetic apertures via a growth-curve analysis (Stetson 1990). All transformations from the WFPC2 instrumental system to the standard ground-based  $V, I$  system were performed with a version of the program CCDSTD (see Stetson 1993). Because the edges of the pyramid mirror in WFPC2 are imaged onto the photosensitive areas of the four camera CCDs, this analysis will be confined to that area of each chip which is almost certainly unvignetted; this has been taken to be  $75 < X, Y < 800$  in the three WFC chips, and  $100 < X, Y < 800$  in PC.

The ground-based Johnson  $V$  and Kron-Cousins  $I$  magnitudes which will be used for calibrating WFPC2 are taken from Walker (1994) for  $\omega$  Cen, and from my own analysis of ground-based data for NGC 2419. The photometry for the latter cluster is based upon 68  $V$  and 62  $I$  frames obtained during the course of 14 nights in six observing runs. The images were taken with the Kitt Peak 4m and 2.1m telescopes, the Canada-France-Hawaii Telescope (data obtained through the courtesy of the Canadian Astronomy Data Centre), and the Isaac Newton Telescope (data obtained through the courtesy of the Isaac Newton Group Archive), and have been rigorously transformed to the photometric system of Landolt (1992) as part of an ongoing program that has now homogenized photometric data from over 40 individual observing runs.

NGC 2419 is a massive, rich globular cluster located about 100 kpc away, and the field is quite crowded under groundbased seeing conditions. Therefore the HST imagery was examined to identify stars that appear to be minimally crowded. Wherever possible, a star identified in the groundbased images was cross-identified with a star detected in the WFPC2 data. Then the groundbased photometry was differentially corrected for those neighbors that were found in the HST images but were *not* identified and accounted for in the analysis of the groundbased data. Any star that required a blending correction in

excess of 0.1 mag was rejected as a potential standard. As the analysis proceeded, any star in either  $\omega$  Cen or NGC 2419 for which the mean of the calibrated HST photometry differed from the mean of the groundbased data by more than 0.3 mag in either filter was likewise discarded, and the solutions were redone until no further rejections were required.  $\omega$  Cen stars that were rejected at this stage were Walker numbers 1, 9, 24, 48, 49, 57, 60, 77, 99, 129, 139, 152, 154, 174, 196, 203, 238, 240, 243, 247, 248, 261, 274, and 275; this left 184  $\omega$  Cen stars for which the groundbased and HST photometry were concordant to within  $\pm 0.3$  mag. Fifteen of 366 stars in NGC 2419 were similarly discarded.

It may be argued that the inclusion of stars with such large standard errors would vitiate any delicate photometric analysis. However, this should not be a serious problem. In the analyses that follow all observations are weighted in accordance with their inferred standard errors, which are fairly well known from the photon statistics and repeatability from multiple images. Then a robust version of least squares is used (see Stetson 1989) which permits the solution to follow the main trend of the data without being unduly influenced by outliers. Inclusion of faint stars is necessary to provide the needed leverage on the magnitude dependence of the charge loss, and a more strict censoring of the data might introduce bias rather than reduce it. In addition, most stars were eventually imaged at many different locations on the various chips. A star whose photometric errors give a semblance of a large charge loss when imaged at a high value of  $X$  or  $Y$  would produce a cancelling effect on other occasions when it appeared at low column or row numbers. As in the differential WH97 study, then, gradients in the photometric zero point across the face of the chips, and variations of those gradients with sky brightness and stellar magnitude will not be sensitive to the accuracy of the groundbased magnitudes. Prior knowledge of the standard photometric magnitudes will be useful only in testing for the presence of position-independent photometric non-linearities, and those tests alone will be affected by uncertainty in the groundbased results.

The present data set will be analysed in three ways: (1) assuming that charge-transfer losses are negligible; (2) correcting the observed stellar fluxes according to the precepts of WH97; and (3) solving for a new numerical model of the charge loss as a function of position, stellar brightness, and sky brightness simultaneously with the determination of the photometric zero points. The results of these three analyses will be presented in §§3.1, .2, and .3, respectively, for the data obtained at a camera temperature of  $-88^{\circ}\text{C}$ . A briefer discussion of the data obtained at the warmer temperature will be presented in §4.

The fundamental assumptions of the present analysis are:

1. The charge-transfer inefficiency affects the gain = 7 and the gain = 14 observations identically, provided care is taken to evaluate the charge loss in units of electrons.
2. The inefficiency is the same for F555W and F814W.
3. The size of the effect has not evolved significantly between 1994 May and 1997 November.
4. The charge loss may be significantly different at a camera temperature of  $-76^{\circ}\text{C}$  as opposed to  $-88^{\circ}\text{C}$ .

WH97 did not require assumptions (1), (3), or (4) because all their observations were obtained on a single date with a single gain setting and camera temperature. Our assumption (1) follows from the hypothesis that the charge transfer inefficiency is completely the result of physical processes within the body of the CCD, and not from subsequent effects that take place during amplification and digitization. Assumptions (2) and (3) are made primarily for simplicity and ease of modifying existing software to perform the present analysis, but the work of WH97 is relevant for assessing the validity of assumption (2), at least. While they found that the gross correction for lost charge does appear to depend upon the filter — the

corrections being the greatest at short and long wavelengths and being least for the F555W and F675W filters — they noted, “This is probably because the chips are more efficient at these wavelengths [*i.e.*, near 555 and 675 nm], hence the background is higher. The higher background appears to reduce the CTE loss...” Thus, when proper quantitative account is taken of the apparent dependence of charge loss on background brightness level, WH97 suggest that the photometric correction does not depend heavily on bandpass. In any case, the validity of assumptions (2) and (3) can be checked *ex post facto* once the average baseline effect of charge-transfer inefficiency has been calibrated and removed. As a result of assumption (4), I have performed separate and independent analyses for the colder and warmer camera temperatures.

### 3. A New Analysis of Charge Loss Effects — Computations

#### 3.1. No corrections

A least-squares fit of the basic transformation equations to the images of 36,234 stars recorded in the cold-camera observations of  $\omega$  Cen and NGC 2419 yielded the photometric zero points listed in Table 1. As mentioned above, the color coefficients derived by Holtzman *et al.* (1995b) were imposed as givens. Specifically,

$$F555W = V + A_V + 0.052 \times (V - I) - 0.027 \times (V - I)^2$$

$$F814W = I + A_I + 0.062 \times (V - I) - 0.025 \times (V - I)^2.$$

The first part of the table gives the zero point for each chip/filter combination based upon the full set of observations obtained with electronics bay 3 (exclusively short exposures of the  $\omega$  Cen field), and the full set with electronics bay 4 (a combination of short exposures of  $\omega$  Cen and both short and long exposures of NGC 2419). In the second part of the table, electronics bay 4 zero points are presented for the short  $\omega$  Cen exposures, the short

Table 1



NGC 2419 exposures, and the long NGC 2419 exposures considered separately. All of these derived zero points are tabulated in detail because they will be used below to test the validity of the various correction schemes.

The calibration residuals  $\delta(\text{magnitude})$  resulting from the 16 combined solutions (2 gain settings  $\times$  2 filters  $\times$  4 chips, corresponding to the zero points listed in Table 1a) were all merged into a single file; the sense of the residual is (observed instrumental magnitude) *minus* (magnitude predicted from the standard-system indices and the mean transformation

Fig. 1 equations). Figure 1 shows the individual residuals plotted versus (top)  $X$  coordinate on the chip, (middle)  $Y$  coordinate on the chip, and (bottom) raw instrumental magnitude  $m$  ( $= \text{constant} - 2.5 \log[\text{number of stellar photoelectrons within a radius of } 0''.5]$ ); for clarity, only unsaturated stars where the combined uncertainty of the ground-based standard magnitude and the WFPC2 instrumental magnitude is less than 0.05 mag have been plotted. It is apparent that there are significant residual trends with both the  $Y$  and  $X$  coordinates, but no systematic nonlinearity with magnitude is obvious. To provide a more quantitative, albeit still crude, measure of the magnitude of these effects, a robust, weighted least-squares surface of the form

$$\delta = a + \frac{\partial \delta}{\partial X} \cdot X + \frac{\partial \delta}{\partial Y} \cdot Y + \frac{\partial \delta}{\partial m} \cdot m + \frac{\partial^2 \delta}{\partial X \partial m} \cdot X \cdot m + \frac{\partial^2 \delta}{\partial Y \partial m} \cdot Y \cdot m + \frac{\partial \delta}{\partial T}$$

was fitted to all 36,234 fitting residuals. The natural-system position variables are  $X$  and  $Y$ ,  $m$  is the instrumental magnitude as defined above, and  $T$  is the date of observation, measured in years from Heliocentric Julian Date 2,450,000.0. To place the amplitude of the position and magnitude trends in a comfortable set of units, I take the maximum displacement of any given well-measured star from the mean of all stars to be  $|\Delta X| < 400$  px,  $|\Delta Y| < 400$  px,  $|\Delta m| < 2.5$  mag. From the least-squares fit I estimate the maximum photometric consequences of the neglected charge-loss corrections to be

$$\frac{\partial \delta}{\partial X} \cdot (400 \text{ px}) = +0.0150 \pm 0.0006 \text{ mag},$$

$$\begin{aligned}
\frac{\partial \delta}{\partial Y} \cdot (400 \text{ px}) &= +0.0154 \pm 0.0006 \text{ mag}, \\
\frac{\partial \delta}{\partial m} \cdot (2.5 \text{ mag}) &= +0.0142 \pm 0.0004 \text{ mag}, \\
\frac{\partial^2 \delta}{\partial X \partial m} \cdot (400 \text{ px}) \cdot (2.5 \text{ mag}) &= +0.0038 \pm 0.0008 \text{ mag}, \\
\frac{\partial^2 \delta}{\partial Y \partial m} \cdot (400 \text{ px}) \cdot (2.5 \text{ mag}) &= +0.0150 \pm 0.0008 \text{ mag}.
\end{aligned}$$

The positive signs of the first three coefficients, representing the linear dependence on position and magnitude, indicate that the instrumental magnitude is too large, *i.e.*, the star is measured too faint with respect to the average zero-point for all stars taken together, when the  $X$  coordinate is large, the  $Y$  coordinate is large, or the star is faint (large  $m$ ) — all in accordance with the simple predictions of the charge-loss model. The positive signs of both second derivatives demonstrate that the effect of charge loss is further compounded for faint stars at large  $X$  and  $Y$  positions. For a star in a typical exposure, any one of these neglected corrections can cause a systematic error of no more than about 0.015 mag, which corresponds to a root-mean-square error of about 0.01 mag. A star in the wrong corner of position-magnitude space could, however, be subject to an error more than four times larger. Note in particular that the result for  $\frac{\partial \delta}{\partial m} = (+5.69 \pm 0.17) \times 10^{-3}$  implies a stretching of the instrumental magnitude scale, on average: faint stars are measured too faint compared to bright ones, by about 0.03 mag per 5 magnitudes (an approximate figure for the effective dynamic range of WFPC2).

The remaining coefficient determined from the least-squares fit to the residuals is

$$\frac{\partial \delta}{\partial T} = +0.0004 \pm 0.0002 \text{ mag yr}^{-1}.$$

The positive sign of the result indicates that for fixed true-system magnitudes, the observed instrumental magnitudes are becoming larger, *i.e.*, fainter, as time passes. However, with an indicated rate  $< 0.001 \text{ mag yr}^{-1}$ , this secular change is not very important even over the more than 3.5 years over which the cold-camera data were obtained.

### 3.2. The WH97 corrections

In applying the WH97 corrections to the present data sets, all star and sky fluxes were converted to units of electrons, assuming gain values of identically  $7.0$  or  $14.0 \text{ e}^-/\text{DN}$ , to facilitate combining data obtained with either of the two electronics bays. Since I will be calibrating small, differential magnitude corrections directly from stellar observations, minor differences between the postulated and actual gain factors will not seriously damage the analysis. The numerical coefficients of the WH97 equations were adjusted to represent fluxes expressed in units of electrons rather than electronics bay 4 data numbers.

As noted above, the logarithm of the sky brightness varies rapidly as the sky brightness approaches zero, and is undefined for any non-positive estimate of the sky flux. In fact, Table 1 of WH97 indicates that seven of their 44 digital images had inferred median sky-brightness values,  $BKG_{\text{blank}}$ , that were negative; a further 18 images had positive median brightness values that were less than  $0.5 \text{ DN px}^{-1}$ , where a small inaccuracy in  $BKG_{\text{blank}}$  begins to lead to a significant change in  $\log BKG_{\text{blank}}$ . WH97 make no explicit mention of how images like these are to be treated in their methodology. The electron-trap model of the charge-transfer inefficiency predicts that a realistic stellar image would lose only a finite number of electrons even in the limit of a hypothetical exposure with a zero effective background (a short exposure of bright stars through a narrow filter, for instance). Therefore, it is apparent that some modification must be made to the formulae so that the predicted photometric correction approaches a finite constant value as the estimated background brightness reaches (and, in the presence of noise, possibly passes through) zero. In the present analysis I do this by simply “softening” the inferred sky brightness at low values:

$$BKG_{\text{adopted}} = \left\{ (1 \text{ e}^-)^2 + [\max(0, BKG_{\text{observed}})]^2 \right\}^{\frac{1}{2}}. \quad (1)$$

(Please note that in the present analysis, the units of  $BKG$  are electrons, not DN as in

the WH97 study.) The softening constant,  $1\text{ e}^-$ , has been adopted arbitrarily, and has as its sole justification the fact that it is better than doing nothing. Fig. 9 of WH97 indicates that the fraction of charge lost from a stellar image continues to increase down to  $\log[BKG(DN)] \sim -1$ , or  $BKG \sim 0.7\text{ e}^-/\text{pixel}$ , but diffuse sky fluxes below this have not been sampled. The imposition of this minimum inferred sky brightness means that all frames where the diffuse sky brightness is small compared to  $1\text{ e}^-/\text{pixel}$  will be subject to similar, finite, photometric corrections. Henceforth in this paper, the unqualified symbol  $BKG$  will refer to  $BKG_{\text{adopted}}$  as defined in Eq. 1.

Having made this one modification to the WH97 photometric corrections, I then recomputed the cold-camera zero points for the various combinations of gain factor, chip, and filter, arriving at the results shown in Table 2. I forgo plotting the residuals from these solutions, but the numerical correlations with the various independent variables are:

$$\begin{aligned}
\frac{\partial\delta}{\partial X} \cdot (400\text{ px}) &= +0.0109 \pm 0.0006\text{ mag} \\
\frac{\partial\delta}{\partial Y} \cdot (400\text{ px}) &= -0.0017 \pm 0.0006\text{ mag} \\
\frac{\partial\delta}{\partial m} \cdot (2.5\text{ mag}) &= +0.0026 \pm 0.0004\text{ mag} \\
\frac{\partial^2\delta}{\partial X\partial m} \cdot (400\text{ px}) \cdot (2.5\text{ mag}) &= -0.0044 \pm 0.0008\text{ mag} \\
\frac{\partial^2\delta}{\partial Y\partial m} \cdot (400\text{ px}) \cdot (2.5\text{ mag}) &= +0.0109 \pm 0.0008\text{ mag} \\
\frac{\partial\delta}{\partial T} &= +0.0005 \pm 0.0002\text{ mag yr}^{-1}
\end{aligned}$$

Thus, the WH97 corrections operate in the right direction to reduce the size of the maximum systematic error induced by the electron traps, but they do not eliminate the errors entirely, at least for the present data set: some of the charge-loss effects are slightly over-corrected, others are significantly under-corrected. Most notably, in these data the amount of charge lost in the serial register (the  $X$  direction) appears to be larger than estimated by WH97, as is the dependence of the  $Y$ -coordinate ramp on instrumental magnitude (which has been

set to zero in their model). As a result, a maximum systematic error in excess of 0.02 mag is still possible for stars in an unfortunate location in  $(X, Y, m)$  space in an average exposure.

### 3.3. New model corrections

For internal consistency, unlike WH97 I adopt symmetric, exponential-of-a-logarithm, formulations for the charge-transfer losses in both  $X$  and  $Y$  as functions of both star and sky flux. In doing this, I claim no superior knowledge of the detailed physics of charge loss, but rather follow WH97’s lead in postulating a simple, phenomenological, numerical model for the required photometric corrections. At the same time, in reconsidering the WH97 equations, I have tried to improve on some of the aforementioned features of their formulation.

In particular, I have added a term to the formula which allows for the possibility of a charge loss which is independent of the image’s position on the chip. In doing this, I have arbitrarily assumed that any charge loss which *is* independent of position will have precisely the same dependence on sky brightness and stellar flux as the  $Y$ -dependent ramp correction. Again, this assumption is arbitrary and has been made to reduce the number of independent coefficients that must be determined; it is physically reasonable provided that the electron traps contributing to any position-independent charge loss are physically similar to those that produce the well-documented  $Y$  photometric ramp in the body of the detector, which may be different from the traps that produce the less well-understood  $X$ -dependent charge losses that probably occur in the serial register. Of course, if it should happen that there are no position-independent effects, the least-squares analysis will allow the coefficient of the constant term to assume a negligibly small value.

Finally, rather than expressing the equations in terms of the image positions and the

star and sky brightness in absolute terms, I consider expansions about “typical” values of these variables. This makes the various terms in the formulae more nearly independent of each other, so that the least-squares solution is less ill-determined, and also leads to derived standard errors of the coefficients that can be understood in a simple and direct way.

With  $BKG$  representing the softened sky flux in  $e^-/\text{pixel}$ ,  $CTS$  representing the stellar flux within a  $0''.5$  (radius) aperture in  $e^-$ , and  $X$  and  $Y$  the position of the star image in the natural coordinate system of the chip, the adopted numerical model for the photometric corrections is:

$$\Delta X = \frac{X - 425}{375}; \quad (2)$$

$$\Delta Y = \frac{Y - 425}{375}; \quad (3)$$

$$sky = \log_{10} [BKG] - 1; \quad (4)$$

$$star = \log_{10} [CTS] - 4; \quad (5)$$

$$Y\text{-CTE} = c_1 + c_2 \times sky + c_3 \times star; \quad (6)$$

$$X\text{-CTE} = c_4 + c_5 \times sky + c_6 \times star; \quad (7)$$

$$C = 1 + 0.01 \times (c_7 + \Delta Y) \times e^{Y\text{-CTE}} + 0.01 \times \Delta X \times e^{X\text{-CTE}}. \quad (8)$$

If  $m$  represents the measured stellar magnitude relative to whatever zero point, then

$$m(\text{corrected}) = m(\text{observed}) - 2.5 \log C. \quad (9)$$

This model is not as formidable as it looks.  $(\Delta X, \Delta Y) = (0, 0)$  is equivalent to  $(X, Y) = (425, 425)$  — a point near the center of the unvignetted area on each of the WFPC2 CCDs — while  $\Delta X = \pm 1$ ,  $\Delta Y = \pm 1$  refer to points near the edges of the photometrically reliable field. The peculiar combination of natural and base-10 logarithms and exponents used here is not entirely whimsical; for me, at least, it facilitates performing order-of-magnitude estimates in the head. For instance, the constant  $c_7 e^{c_1}$  approximately represents the fraction of charge lost (expressed in percent) from a star image containing

10,000 electrons near the effective center of an image that has a sky surface brightness of  $10\text{ e}^-/\text{pixel}$ . The constants  $\pm e^{c_1}$  and  $\pm e^{c_4}$  represent the degree to which such a star would lose more or less charge if measured near the edge of the field rather than near the center as a result of, respectively, the  $Y$  and  $X$  ramps. For star images containing either 100,000 or 1,000 electrons, these corrections would differ by  $e^{\pm c_3}$  and  $e^{\pm c_6}$  percent, respectively. Likewise, for sky values of 100 or  $\lesssim 1\text{ e}^-/\text{pixel}$  (“ $\lesssim$ ” because of the softening), the corrections for a 10,000-electron star image would differ by  $e^{\pm c_2}$  and  $e^{\pm c_5}$  percent. Encoding the corrections as proportional to  $\exp[\log(CTS)]$  and  $\exp[\log(BKG)]$  ensures that they will go asymptotically — although not necessarily quickly — to zero as  $CTS \rightarrow \infty$  or  $BKG \rightarrow \infty$ , as long as  $c_2$ ,  $c_3$ ,  $c_5$ , and  $c_6$  are all less than or equal to zero. At the other extreme, the softening of the sky brightness ensures that the correction approaches a constant value for any given star in the limit as the background flux becomes negligible. No corresponding numerical protection in the limit of negligibly small stellar flux is required, since the apparent magnitude of a statistically insignificant star is usually of little astronomical interest.

A copy of the computer program CCDSTD (Stetson 1993) was modified to yield numerical values and uncertainties for the seven model constants  $c_1, \dots, c_7$ , as well as the zero points of the transformation from instrumental to standard magnitudes. As before, the 16 separate zero points  $A_V$  and  $A_I$  were computed for the four chips and the two gain settings (eight values for  $A_V$  and eight for  $A_I$ ), based on the cold (camera temperature =  $-88^\circ\text{C}$ ) data only. The same gain =  $7\text{ e}^-/\text{DN}$  zero points were assumed to apply for the  $\omega\text{ Cen}$  data and both short and long exposures of NGC 2419. At the same time, the cold data for all four chips, both filters, both gain settings, and both clusters were used to determine a single, unique set of values  $c_1, \dots, c_7$ . The numerical results of this exercise

Table 3 were the zero points listed in Table 3a and

$$\begin{aligned}
c_1 &= +0.629 \pm 0.021; \\
c_2 &= -0.558 \pm 0.020; \\
c_3 &= -0.593 \pm 0.014; \\
c_4 &= +0.704 \pm 0.027; \\
c_5 &= +0.027 \pm 0.032; \\
c_6 &= -0.359 \pm 0.041; \\
c_7 &= +1.191 \pm 0.018.
\end{aligned}$$

All of these terms  $c_i$  appear to be highly significant, with the sole exception of the sky dependence of the  $X$ -coordinate ramp ( $c_5$ ): for a ten-fold change in the sky brightness (*e.g.*, from  $10 \text{ e}^-/\text{pixel}$  to either 1 or  $100 \text{ e}^-/\text{pixel}$ ) the required correction changes by only  $0.03 \pm 0.03\%$  at the right and left edges of the field, which abundantly justifies the neglect of this term by WH97. However, a dependence of the  $Y$  ramp on stellar flux ( $c_3$ ), which WH97 also omitted, appears to be strongly supported by these data.

According to this model, a star image consisting of  $10,000 \text{ e}^-$  near the center of an image with a sky brightness of  $10 \text{ e}^-/\text{pixel}$  loses approximately  $c_7 e^{c_1} = 1.191 e^{+0.629} = 2.2\%$  of its electrons; at  $Y = 50$  and  $Y = 800$  it loses  $0.191 e^{+0.629} = 0.4\%$  and  $2.191 e^{-0.378} = 4.1\%$  yielding, in this case, a ramp of about  $3.8\%$  per 750 pixels or  $4.0\%$  per 800 pixels. In the hypothetical row  $Y = 0$  the same star would lose  $\left[\left(\frac{-425}{375}\right) + 1.191\right] e^{+0.629} = 0.1\%$ , so a position-independent contribution to the total correction, while apparently statistically significant, is clearly not very important. Decreasing the sky brightness by a factor of ten would increase the  $Y$  ramp by a factor  $e^{+0.558} \approx 1.75$ , to about  $7.0\%$  per 800 pixels. For a star 2.5 magnitudes brighter, with  $100,000 \text{ e}^-$  in its image, the  $Y$  ramp would be smaller by a factor  $e^{-0.593} \approx 0.55$ , yielding  $2.2\%$  per 800 pixels for  $10 \text{ e}^-/\text{pixel}$  in the sky, or  $3.9\%$  per 800 pixels for a sky brightness of  $1 \text{ e}^-/\text{pixel}$ . The numerical correlations between the fitting



residuals and position and magnitude are:

$$\begin{aligned}
\frac{\partial \delta}{\partial X} \cdot (400 \text{ px}) &= -0.0018 \pm 0.0006 \text{ mag} \\
\frac{\partial \delta}{\partial Y} \cdot (400 \text{ px}) &= -0.0014 \pm 0.0006 \text{ mag} \\
\frac{\partial \delta}{\partial m} \cdot (2.5 \text{ mag}) &= -0.0066 \pm 0.0004 \text{ mag} \\
\frac{\partial^2 \delta}{\partial X \partial m} \cdot (400 \text{ px}) \cdot (2.5 \text{ mag}) &= -0.0007 \pm 0.0008 \text{ mag} \\
\frac{\partial^2 \delta}{\partial Y \partial m} \cdot (400 \text{ px}) \cdot (2.5 \text{ mag}) &= -0.0035 \pm 0.0008 \text{ mag}
\end{aligned}$$

These are not identically equal to zero because, (a) these linear correlations do not have the same functional forms as the terms defined in the least-squares photometric solution, and (b) in the two separate robust least-squares fits — one for the model parameters plus independent zero points for 16 distinct data sets, and one for the correlations between residuals and positions and magnitudes for all 16 data sets considered together — the weighting schemes cannot be perfectly reproduced: the degrees of freedom are different. In particular, in fitting the correction model no allowance was made for a separate trend of photometric error with magnitude independent of position on the chip, so if such a trend is present it cannot be perfectly compensated by the model. As a result, the single most significant residual correlation is  $\frac{\partial \delta}{\partial m} = (-2.64 \pm 0.17) \times 10^{-3}$ . The sign of this correlation has changed from the uncorrected solutions, indicating that trend of increasing fractional charge loss with decreasing stellar flux has been overcorrected, on a global average over the face of the four chips. The corrected magnitude scale is now apparently compressed by  $-0.013$  mag per 5 magnitudes, as compared to the groundbased results. I believe that this level of systematic error is small compared to other unavoidable biases endemic to photometric measurements of very faint stars (see, *e.g.*, Stetson & Harris 1988, §V(b)), and it is unlikely that a much more satisfactory calibration can be derived from the present data. Certainly, in view of the crowding conditions in these fields, I am unable to guarantee that the ground-based photometry is itself linear to this degree of accuracy. Additional

well-established, deep, groundbased photometric sequences in other star fields targeted by HST, such as the Palomar-type globular clusters and fields in the Magellanic Clouds, would be most welcome additions to the study of this problem. Still, after application of this set of corrections to the WFPC2 data, the maximum systematic errors associated with the purely positional variables  $Y$  and  $X$  are now well under 1%, at least averaged over the present data set.

The secular trend of the photometric residuals with time that remains after applying these corrections is

$$\frac{\partial \delta}{\partial T} = +0.0012 \pm 0.0002 \text{ mag yr}^{-1}.$$

This is larger than was estimated in §3.1 — presumably because in the uncorrected data the mean trend with time was partially masked by scatter resulting from the neglect of the charge-loss effects — but over the 3.5 years of available WFPC2 data this still implies a maximum departure from the mean zero points of order 0.002 mag at the two ends of the time interval covered.

### 3.4. Summary of the cold-camera data

There are several additional sanity checks which can be derived from these data. For instance, if the corrections truly are valid, then the photometric zero point for a given chip/filter combination should be independent of exposure time. We can perform this test with the short and long exposures of NGC 2419; I omit the  $\omega$  Cen exposures from consideration here because this eliminates confusion produced by any possible differences between the ground-based photometric systems for the two clusters. The four chips and two filters provide us with eight independent measures of the (short – long) zero-point difference (data listed in Tables 1b, 2b, 3b). Taking the unweighted mean of the eight (short – long) zero-point differences, I find net values of  $+0.0243 \pm 0.0087$  (standard error

of the mean; 0.0245 standard deviation of one difference) based on the reductions with no photometric corrections;  $+0.0048 \pm 0.0086$  (s.e.m.; 0.0243 s.d.) with the WH97 corrections; and  $+0.0030 \pm 0.0079$  (s.e.m.; 0.0224 s.d.) with the new corrections derived in §2.3. In other words, the WH97 corrections largely eliminate the perceived difference in zero points between short and long exposures, but the chip-to-chip and filter-to-filter scatter in the differences is not much reduced by the WH97 corrections. The newly derived corrections represent a slight improvement on those of WH97, in that they reduce the residual (short – long) zero-point difference a bit further, and also slightly reduce the chip-to-chip and filter-to-filter scatter. Repeating the experiment with weighted means (after all, the PC1 zero points are based on roughly one-fourth as many stars as those for the wide-field chips) we obtain a mean (short – long) difference of  $+0.0244 \pm 0.0122$  for the uncorrected data;  $+0.0049 \pm 0.0123$  with the WH97 corrections; and  $+0.0033 \pm 0.0110$  with the new corrections.

The gain ratio between Electronics Bay 3 and Electronics Bay 4 may differ from one CCD to the next, but we may expect that the gain will not depend upon the filter with which a given exposure was made. If this is the case, then the difference between the gain = 14 zero point and the gain = 7 zero point should be the same in *V* and *I*. For instance, with no photometric corrections, for chip 1 the *V* zero point from the gain = 14 observations of  $\omega$  Cen is 1.7673 (Table 1a), and the gain = 7 zero point is 0.9974 (Table 1b; again, this test considers the gain = 7 observations for  $\omega$  Cen alone to eliminate the effects of any residual differences between the  $\omega$  Cen and NGC 2419 ground-based photometry), for a gain ratio of 0.7699 mag. The *I*-band gain ratio for the same chip is  $2.6667 - 1.9405 = 0.7262$  mag, and the difference between the *V* and *I* gain ratios is 0.0437 mag, rather than the expected zero. Each separate calibration produces four values of this gain-ratio difference, from the four chips. The unweighted root-mean-square value of these four differences is: 0.0245 mag for the uncorrected reductions, 0.0258 mag with the WH97 corrections, and 0.0285 mag

with the new corrections.

For each filter, the zero points of the gain = 14 observations should be the same in the four chips, because the flat-field observations were made with the gain = 14 electronics and the flat fields were normalized over the four chips taken together so that surface brightnesses measured in the different chips would be restored to a common system. The standard deviations of the individual chips about the unweighted mean zero points for the two filters (eight observations, six degrees of freedom) are 0.0114 mag for the uncorrected reductions, 0.0098 mag with the WH97 corrections, and 0.0142 mag with the new corrections.

The tests described in this section are quite indirect, and rely on some untested assumptions for their validity: that gain ratio is independent of wavelength, for instance. Therefore these results can be no more than suggestive. There is a hint that the WH97 corrections do better than the new ones when applied to the  $\omega$  Cen data alone, as in the gain-ratio test and the test assuming the equality of the gain = 14 zero points. The new corrections seem to do better when the NGC 2419 observations are added to the sample, as in the short-long test here, and in the global fitting residuals discussed in §§3.2 and .3. If the self-consistency tests of this section have any meaning at all, it is that the errors in the present data set are not totally random, but rather contain unmodeled systematic components as well. For instance, the photometric zero points may vary erratically with time, or with the history of previous exposures, or with some other variable not included in the phenomenological model. If this is true, then the standard errors quoted at various places in §3 and in Tables 1–3 — which were estimated simply from the root-mean-square scatter divided by the square root of the number of fitting residuals — are merely attractive fictions; the true errors for any given selected subset of the data may be considerably larger. It appears that the photometric zero point for any given chip/filter combination in any given data set is really externally reliable only to  $\gtrsim 0.01$  mag, regardless of the

standard errors listed in the tables. For instance, the dispersion of zero-point *differences* in the (short – long) test just performed was  $\sim 0.024$  mag, so the typical uncertainty of the zero-points themselves would be smaller by  $\sqrt{2}$ , or  $\sim 0.017$  mag. Similarly, the gain-ratio test involved differences of differences of zero points, with a scatter  $\sim 0.026$ , implying zero points individually reliable to  $\sim 0.013$  mag, while the third test, involving zero points directly, implied a typical external uncertainty in the range  $0.010 - 0.014$  mag.

Whitmore (1998) has conducted an analysis of the time variability of the charge-transfer inefficiency based on seven images of the  $\omega$  Cen standard field obtained with WFPC2 operating at the colder temperature and spanning the dates 1994 April to 1997 June. He concluded that the CTE loss has increased over that period of time, but only for the faintest stars: those containing from 20 to 50 DN within a  $0''.2$  aperture in very short exposures at the  $14 e^-/\text{DN}$  gain setting appeared to lose  $22 \pm 3\%$  of their electrons when clocked out through 800 rows in the detector at the end of that period, as compared to  $3 \pm 3\%$  at the beginning. A flux of 280 to  $700 e^-$  within  $0''.2$  corresponds, on my instrumental magnitude scale, to  $m \approx 18.5$  at gain =  $7 e^-/\text{ADU}$  and  $m \approx 19.25$  at gain = 14. Accordingly, I have selected out the photometric residuals, *after* the application of the new corrections derived in §3.3, for stars with predicted instrumental magnitudes fainter than those limits. For these stars considered separately, I find

$$\begin{aligned} \frac{\partial \delta}{\partial X} \cdot (400 \text{ px}) &= -0.0026 \pm 0.0007 \text{ mag} \\ \frac{\partial \delta}{\partial Y} \cdot (400 \text{ px}) &= -0.0028 \pm 0.0007 \text{ mag} \\ \frac{\partial \delta}{\partial T} &= +0.0025 \pm 0.0002 \text{ mag yr}^{-1} \end{aligned}$$

(Systematic variations of the residuals with stellar brightness are not worth investigating in a sample with this limited range of instrumental magnitude.) For these faint stars, it seems that the new corrections overcompensate a bit for the mean rate of charge loss with  $X$  and  $Y$  position on the chip — the net trends are slightly negative, indicating that the corrected

magnitudes are a little too bright at positive values of  $\Delta X$  and  $\Delta Y$  — but the maximum error is  $\ll 1\%$  and the r.m.s. error averaged over the face of the chip is  $\sim 0.0016$  mag in both  $X$  and  $Y$ . The residuals for these very faint star images do show a systematic positive trend with time, as found by Whitmore: the mean residual increases at a rate of  $0.0025$  mag  $\text{yr}^{-1}$ , for a total net difference of  $0.009$  mag over the 3.5 years spanned by the current data set for a faint star located near  $(X, Y) = (425, 425)$  or, equivalently, for the average of many stars scattered uniformly over the detector field. Both the overcorrection of the  $X$  and  $Y$  ramps and the apparent secular increase of the charge loss with time are much smaller than the random Poisson noise for any star image containing  $280\text{--}700\text{ e}^-$ . Indeed, the random observational errors for star images this faint are almost always larger than  $0.05$  mag when all error contributors are considered. That is why these stars are essentially absent from Fig. 1 where, for reasons of clarity, only the more precise measurements have been plotted. The unmodeled systematic trends of these faint-star residuals are also much smaller than the systematic statistical effects discussed, *e.g.*, by Stetson & Harris (1988). Still, while these remaining systematic effects are unimportant on a star-by-star basis, the reader should be aware that ensemble average magnitudes for large numbers of very faint stars observed in short exposures may be subject to these additional (relatively minor) sources of systematic error.

Whitmore further states that for star images containing at least  $2800\text{ e}^-$  within  $0''.2$  (radius) the rate of increase of charge loss with time is negligible, even in exposures with very low background levels. It is probably safe to assume that the secular evolution of the charge losses will be doubly negligible in images that contain significant background levels, and that one generic set of charge-loss corrections will be reasonably valid over the 3–3.5 years spanned by existing studies. The results presented here certainly seem to bear that conclusion out.

#### 4. Warm Data

WFPC2 was operated at a camera temperature of  $-76^\circ$  C from installation in 1993 December until 1994 April 23. Between 1994 January 11 and April 21 the  $\omega$  Centauri standard field was observed a number of times in F555W employing both electronics bays, but observations in F814W are only available for the gain = 14 electronics. Determining the mean photometric zero points in the usual way, under the assumption of no charge loss, we arrive at the fitting residuals shown in Figure 2. There are comparatively few observations from the short period of time when the camera was operated at the higher temperature (14,521 residuals are shown in Fig. 2), and the data do not span the chips nearly as well as in the more extensive cold data. It is clear that there is a considerable charge-loss effect in the  $Y$  coordinate, but any systematic trends with  $X$  and magnitude are too small to be seen at this scale.

I have attempted to determine charge-loss coefficients for the warm data as I did for the cold. I quickly found that the solution for the fitting parameter  $c_4$  rapidly diverged to  $-\infty$ , indicating that any charge loss in the serial register is too small to measure even in a statistical sense. In order to get a self-consistent solution, therefore, it was necessary to simplify the problem. Accordingly, I effectively turned off the ramp correction in  $X$  by assigning  $c_4$  a value of  $-20$ , and I also eliminated the possibility of a position-independent charge loss by setting  $c_7$  identically equal to  $\frac{425}{375} = 1.1333$ . The standard robust solution for the remaining three significant terms yielded

$$c_1 = +1.271 \pm 0.035,$$

$$c_2 = -0.449 \pm 0.040,$$

$$c_3 = -0.254 \pm 0.011,$$

plus the zero points listed in Table 4. In a frame with a mean background of  $10\text{ e}^-/\text{pixel}$ , the total amount of charge lost from a 10,000 electron star at  $Y = 800$  ( $\Delta Y = 1$ ) is

$2.1333 e^{1.271} = 7.6\%$ , as compared to  $2.191 e^{0.629} = 4.1\%$  for the cold data. For the warm data, the variation of the charge loss with background level appears marginally less than for the cold data, but the dependence on the brightness of the star is about twice as strong.

## 5. Conclusion

For  $\omega$  Cen, a total of 152 WFPC2 exposures in the F555W filter and 159 exposures in F814W spread over 3.5 years of observations have now been calibrated to a common photometric system. In contrast, Walker’s (1994) groundbased study of  $\omega$  Cen was based on only 12  $V$  and 10  $I$  frames obtained over the course of six nights in 1985, using an early RCA CCD. By combining the HST data with Walker’s it should be possible to get an improved standard sequence in  $\omega$  Cen, “improved” at least in the sense of being

Fig. 3 internally more precise even if not externally more accurate. Figure 3(a) is a  $(V-I, V)$  color-magnitude diagram for Walker’s stars in  $\omega$  Cen, while Fig. 3(b) shows the same stars, but with the present WFPC2 photometry — corrected for charge-transfer inefficiency and transformed to the standard  $V, I$  system using the precepts of §§2.3 and 3 and the zero points of Tables 3 and 4 — averaged together with Walker’s. Given the large body of HST data, it is also possible to define new standard-sequence stars in  $\omega$  Cen. Accordingly, a list of minimally crowded detections in the  $\omega$  Cen standard field was derived from the output of the ALLFRAME reductions. From among these relatively isolated stars, a total of 1,318 were selected which had been measured at least 10 times in each filter, had standard errors of the mean no larger than 0.03 mag in each of  $V$  and  $I$ , and gave no evidence of intrinsic variability in excess of 0.03 mag, root-mean-square, averaged over the two filters. These are shown in Fig. 3(c). (The figure 1,318 includes stars listed by Walker (1994); 1,116 of them are new ones without Walker, Harris, or Woolley identification numbers as tabulated by Walker.)



Fig. 4

Figures 4(a) and (b) show, respectively, the ground-based photometry for NGC 2419, and the *HST*-based photometry averaged together with the ground-based data for the same stars. Since in NGC 2419 I had already selected out a large sample of minimally crowded stars to define the ground-based standard sequence in the first place, there is no need to pick out additional local standards based on the HST data alone.

There is an advantage in re-deriving final sets of zero points based upon these improved, homogenized standard sequences in the two clusters. With most of the stars having been measured on more than one of the four chips during the course of the observations, as well as having been measured in both long and short exposures (in the case of NGC 2419), with the gain = 7 and gain = 14 e<sup>-</sup>/DN electronics (in the case of  $\omega$  Cen), and with the camera operating at both the warmer and colder temperatures ( $\omega$  Cen), any residual systematic errors remaining in the individual data subsets will be diluted when all are averaged together. Add to these considerations the fact that the total number of standards has now been increased from 534 to 1,714 while the random errors have been reduced from a median value of 0.017 mag per star to a median of 0.007 mag per star, and it follows that the derivation of new zero points based on the improved standard sequence will yield photometry that is more homogeneous across the various data sets, even though the reanalysis cannot lead to photometry that is more absolutely correct on the average over all data sets. The final zero points that result from calibration of the CTE-corrected data with the augmented list of standards are given in Table 5. Again, the reader should note that the formal standard errors listed in the table are outrageously optimistic; true uncertainties of order 1% or slightly more are far more realistic. Only additional observations will improve this situation.

Table 5

Application of the present CTE corrections to other WFPC2 data is straightforward. Provided that the reader has stellar positions referred to the natural coordinate system of

each chip ( $1 \leq X, Y \leq 800$ ) and is careful to use the known gain ratio of the observation to convert the instrumental magnitude and some estimate of the diffuse sky brightness in the image to units of electrons, then it is merely necessary to add nine lines of code, corresponding to Eqs. (1)–(9), to whatever software the reader is now using. If, in addition, the reader happens to be following the Key Project precepts on the standardization of the raw images (*e.g.*, the images have been multiplied by 4.0 so that they can be stored as short integers without significant loss of precision; see Stetson *et al.* 1998), then the zero points of Table 5 can be used to convert the corrected half-arcsecond aperture magnitudes to the standard system. If the reader does not use the Key Project precepts, Stetson *et al.* (1998) list the steps necessary to relate these zero points to those of Holtzman *et al.* (1995b). The external reliability of photometry on this system is still probably of order 0.01 mag, since the present zero points represent a compromise among gain 7 and gain 14, warm- and cold-camera, and short- and long-exposure data sets, each of which has zero points individually uncertain at the 0.01–0.02 mag level. Internally, however, the various chips should yield photometry consistent at a level somewhat better than this.

I am extremely grateful to Dr. Jeremy Mould and the entire staff of Mount Stromlo and Siding Spring Observatories for the financial support and hospitality during the time when much of this work was being done. Additional financial support from the Jet Propulsion Laboratory of the California Institute of Technology is also very much appreciated.

## REFERENCES

- Harris, H. C., Hunter, D. A., Baum, W. A., & Jones, J. H. 1993, *AJ*, 105, 1196
- Harris, W. E., *et al.* 1997, *AJ*, 114, 1030
- Holtzman, J. A., Burrows, C. J., Casertano, S., Hester, J. J., Trauger, J. T., Watson, A. M., Worthey, G., 1995b, *PASP*, 107, 1065
- Holtzman, J., *et al.* 1995a, *PASP*, 107, 156
- Landolt, A. U. 1992, *AJ*, 104, 340
- Stetson, P. B. 1989, in *V Advanced School of Astrophysics*, eds. B. Barbuy, E. Janot-Pacheco, A. M. Magalhães, and S. M. Viegas (São Paulo: Univ. de São Paulo)
- Stetson, P. B. 1990, *PASP*, 102, 932
- Stetson, P. B. 1993, in *IAU Coll. 136, Stellar Photometry — Current Techniques and Future Developments*, ed. C. J. Butler & I. Elliot (Cambridge: Cambridge Univ. Press), 291
- Stetson, P. B. 1994, *PASP*, 106, 250
- Stetson, P. B., *et al.* 1999, *AJ*, submitted
- Stetson, P. B., & Harris, W. E. 1988, *AJ*, 96, 909
- Stetson, P. B., *et al.* 1998, *ApJ*, in press
- Walker, A. R. 1994, *PASP*, 106, 828
- Whitmore, B. 1998, *Technical Instrument Report WFPC2 98-01* (Baltimore: STScI)
- Whitmore, B., & Heyer, I. 1997, *Instrument Science Report WFPC2 97-08* (Baltimore: STScI) [WH97]

## FIGURE CAPTIONS

Fig. 1.— Fitting residuals of individual stellar measurements from photometric solutions where no corrections for charge losses have been applied. For clarity, only those measurements with individual uncertainties smaller than 0.05 mag have been plotted, although poorer measurements were included in the numerical analysis. Residuals are plotted against (top)  $X$ -coordinate position in the natural reference frames of the individual chips, (middle)  $Y$ -coordinate position, and (bottom) the instrumental magnitude of the star image, which is related to the number of photoelectrons it contains. Only observations obtained at the colder camera temperature ( $-88^{\circ}\text{C}$ ) are included.

Fig. 2.— As in Fig. 1, except that only observations obtained at the warmer camera temperature ( $-76^{\circ}\text{C}$ ) are included.

Fig. 3.—  $(V, V-I)$  color-magnitude diagrams for the WFPC2 standard field in  $\omega$  Centauri. (a) Walker’s (1994) ground-based measurements. (b) Calibrated WFPC2 photometry averaged with Walker’s for the same stars as in (a). (c) Calibrated WFPC2 photometry for an enlarged sample of stars, as described in the text.

Fig. 4.—  $(V, V-I)$  color-magnitude diagrams for the WFPC2 field in NGC 2419. (a) Ground-based photometry obtained by the author from archival data. (b) Calibrated WFPC2 photometry averaged together with the ground-based data for the same stars as in (a).

Table 1. Chip Zero Points, Assuming No Corrections

Data set	PC1		WF2		WF3		WF4	
a. Combined solutions								
cold, gain = 14, $V$	$1.7673 \pm 0.0029$		$1.7515 \pm 0.0010$		$1.7824 \pm 0.0008$		$1.7593 \pm 0.0012$	
cold, gain = 14, $I$	2.6667	0.0021	2.6534	0.0007	2.6695	0.0010	2.6513	0.0010
cold, gain = 7, $V$	0.9957	0.0023	0.9860	0.0016	0.9922	0.0015	0.9897	0.0016
cold, gain = 7, $I$	1.9728	0.0021	1.8963	0.0012	1.9240	0.0012	1.9473	0.0011
b. Separate solutions, gain = 7								
$\omega$ Cen, $V$	0.9974	0.0030	1.0041	0.0024	1.0056	0.0029	0.9965	0.0024
$\omega$ Cen, $I$	1.9405	0.0031	1.9029	0.0017	1.9035	0.0025	1.9134	0.0016
NGC 2419, short, $V$	0.9979	0.0044	0.9709	0.0026	1.0050	0.0020	0.9899	0.0023
NGC 2419, short, $I$	1.9981	0.0026	1.8929	0.0015	1.9367	0.0014	1.9594	0.0013
NGC 2419, long, $V$	0.9938	0.0061	0.9874	0.0032	0.9591	0.0031	0.9743	0.0037
NGC 2419, long, $I$	1.9468	0.0039	1.8826	0.0038	1.8900	0.0023	1.9224	0.0023

Table 2. Chip Zero Points, Assuming WH97 Corrections

Data set	PC1		WF2		WF3		WF4	
a. Combined solutions								
cold, gain = 14, $V$	1.7264 $\pm$ 0.0026		1.7254 $\pm$ 0.0009		1.7517 $\pm$ 0.0008		1.7326 $\pm$ 0.0014	
cold, gain = 14, $I$	2.6217	0.0021	2.6263	0.0007	2.6355	0.0009	2.6219	0.0011
cold, gain = 7, $V$	0.9610	0.0023	0.9594	0.0016	0.9666	0.0014	0.9649	0.0016
cold, gain = 7, $I$	1.9345	0.0018	1.8640	0.0010	1.8942	0.0010	1.9195	0.0010
b. Separate solutions, gain = 7								
$\omega$ Cen, $V$	0.9571	0.0032	0.9765	0.0023	0.9777	0.0028	0.9680	0.0026
$\omega$ Cen, $I$	1.8967	0.0033	1.8715	0.0014	1.8744	0.0026	1.8795	0.0019
NGC 2419, short, $V$	0.9584	0.0038	0.9379	0.0023	0.9744	0.0018	0.9617	0.0023
NGC 2419, short, $I$	1.9539	0.0021	1.8554	0.0012	1.9024	0.0012	1.9285	0.0011
NGC 2419, long, $V$	0.9734	0.0058	0.9712	0.0032	0.9433	0.0031	0.9672	0.0037
NGC 2419, long, $I$	1.9267	0.0036	1.8668	0.0038	1.8729	0.0024	1.9128	0.0023

Table 3. Chip Zero Points, Assuming New Corrections

Data set	PC1		WF2		WF3		WF4	
a. Combined solutions								
cold, gain = 14, $V$	1.7168 $\pm$ 0.0025		1.7300 $\pm$ 0.0009		1.7556 $\pm$ 0.0008		1.7365 $\pm$ 0.0015	
cold, gain = 14, $I$	2.6096	0.0022	2.6315	0.0007	2.6368	0.0008	2.6275	0.0012
cold, gain = 7, $V$	0.9601	0.0026	0.9678	0.0016	0.9750	0.0014	0.9732	0.0016
cold, gain = 7, $I$	1.9343	0.0019	1.8720	0.0010	1.8991	0.0009	1.9252	0.0009
b. Separate solutions, gain = 7								
$\omega$ Cen, $V$	0.9478	0.0039	0.9850	0.0024	0.9861	0.0028	0.9760	0.0029
$\omega$ Cen, $I$	1.8891	0.0036	1.8776	0.0013	1.8844	0.0024	1.8897	0.0022
NGC 2419, short, $V$	0.9621	0.0039	0.9466	0.0023	0.9824	0.0017	0.9709	0.0022
NGC 2419, short, $I$	1.9542	0.0019	1.8646	0.0012	1.9059	0.0011	1.9337	0.0010
NGC 2419, long, $V$	0.9818	0.0062	0.9791	0.0032	0.9525	0.0030	0.9720	0.0036
NGC 2419, long, $I$	1.9359	0.0041	1.8743	0.0038	1.8815	0.0023	1.9187	0.0023

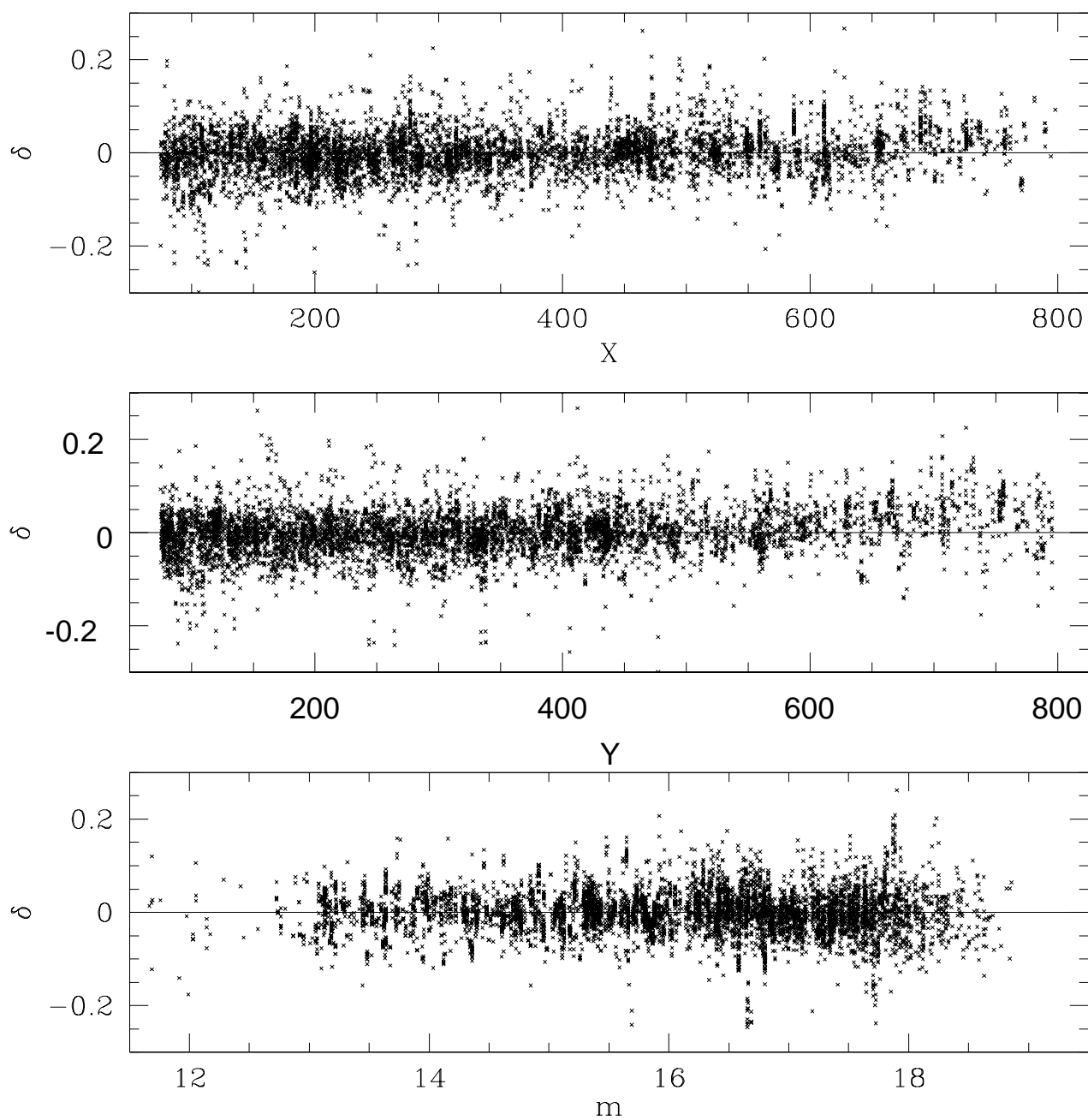
Table 4. Chip Zero Points, Assuming New Corrections

Data set	PC1		WF2		WF3		WF4	
warm, gain = 14, $V$	$1.7805 \pm 0.0019$		$1.7381 \pm 0.0011$		$1.7682 \pm 0.0008$		$1.7612 \pm 0.0009$	
warm, gain = 14, $I$	2.5957	0.0037	2.5852	0.0010	2.6099	0.0008	2.6244	0.0011
warm, gain = 7, $V$	1.0656	0.0047	0.9833	0.0043	1.0298	0.0025	1.0311	0.0037

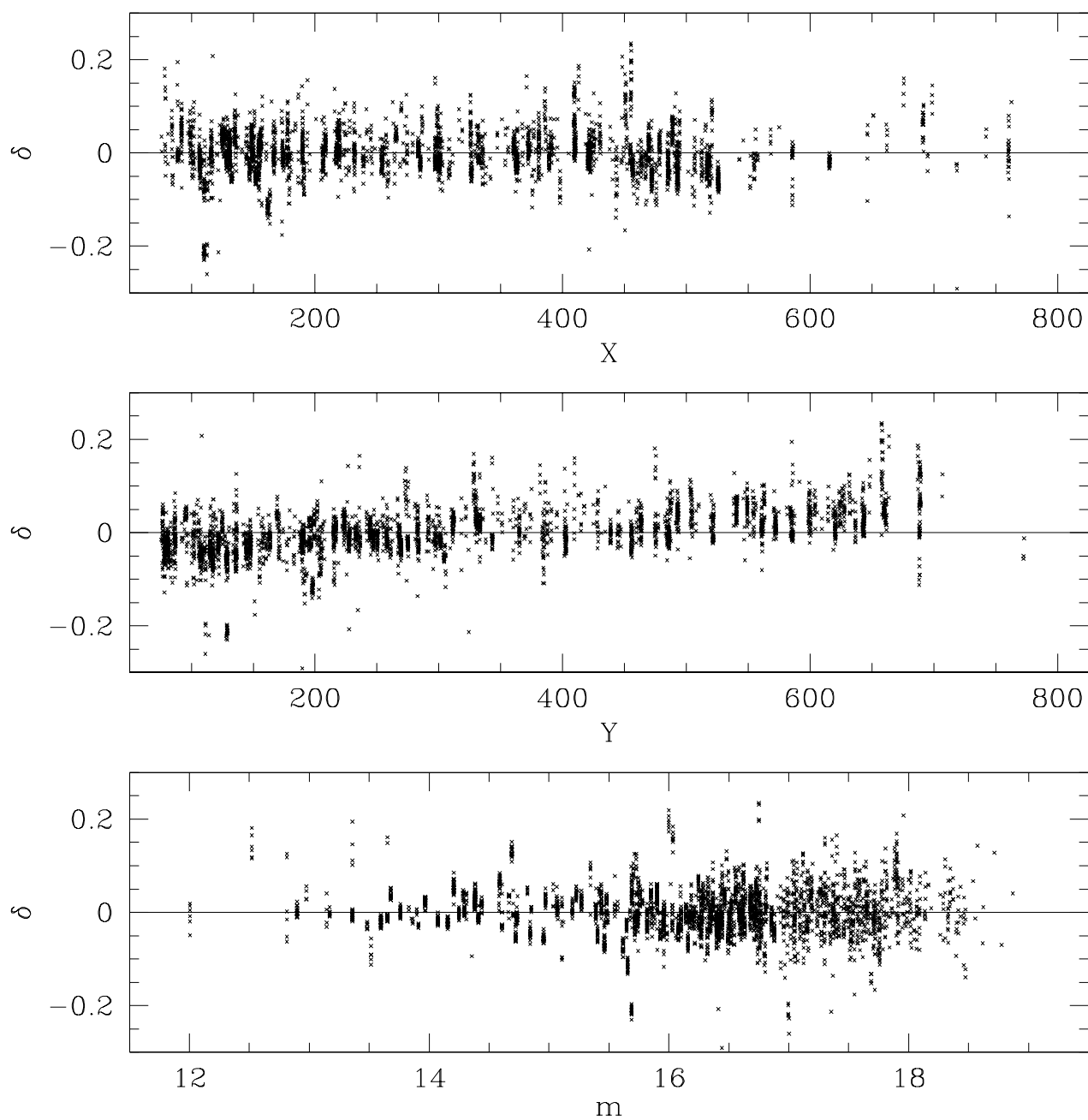
Table 5. Improved Chip Zero Points, Assuming New Corrections

Data set	PC1		WF2		WF3		WF4	
cold, gain = 14, $V$	$1.7222 \pm 0.0010$		$1.7282 \pm 0.0005$		$1.7475 \pm 0.0004$		$1.7285 \pm 0.0005$	
cold, gain = 14, $I$	2.6123	0.0008	2.6313	0.0003	2.6355	0.0004	2.6353	0.0003
cold, gain = 7, $V$	0.9743	0.0012	0.9767	0.0005	0.9820	0.0004	0.9830	0.0005
cold, gain = 7, $I$	1.9088	0.0012	1.8792	0.0004	1.8957	0.0004	1.9140	0.0004
warm, gain = 14, $V$	1.7836	0.0007	1.7441	0.0004	1.7683	0.0004	1.7602	0.0005
warm, gain = 14, $I$	2.5923	0.0013	2.5941	0.0004	2.6122	0.0004	2.6159	0.0005
warm, gain = 7, $V$	1.0643	0.0034	0.9997	0.0016	1.0356	0.0017	1.0264	0.0024

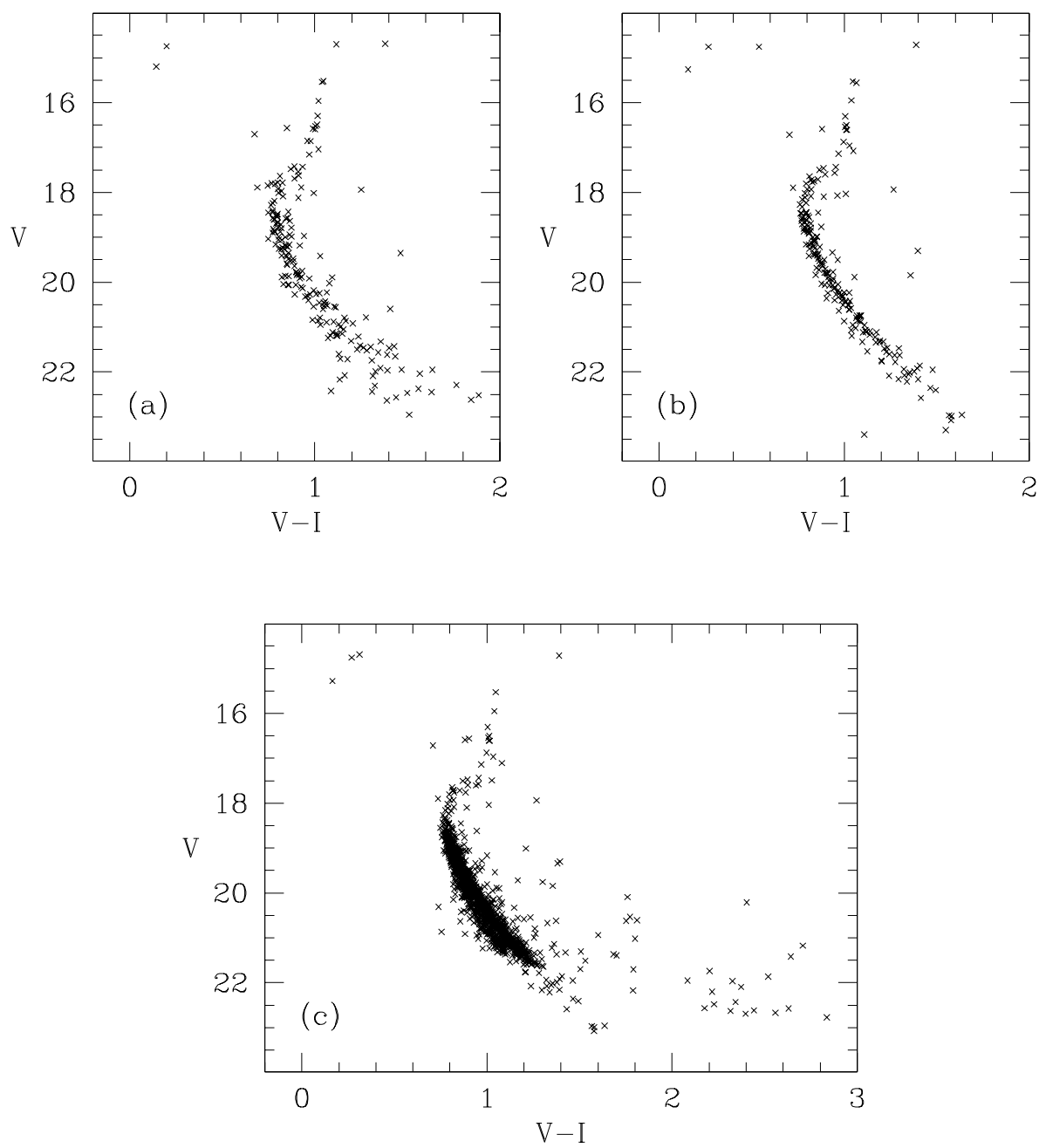




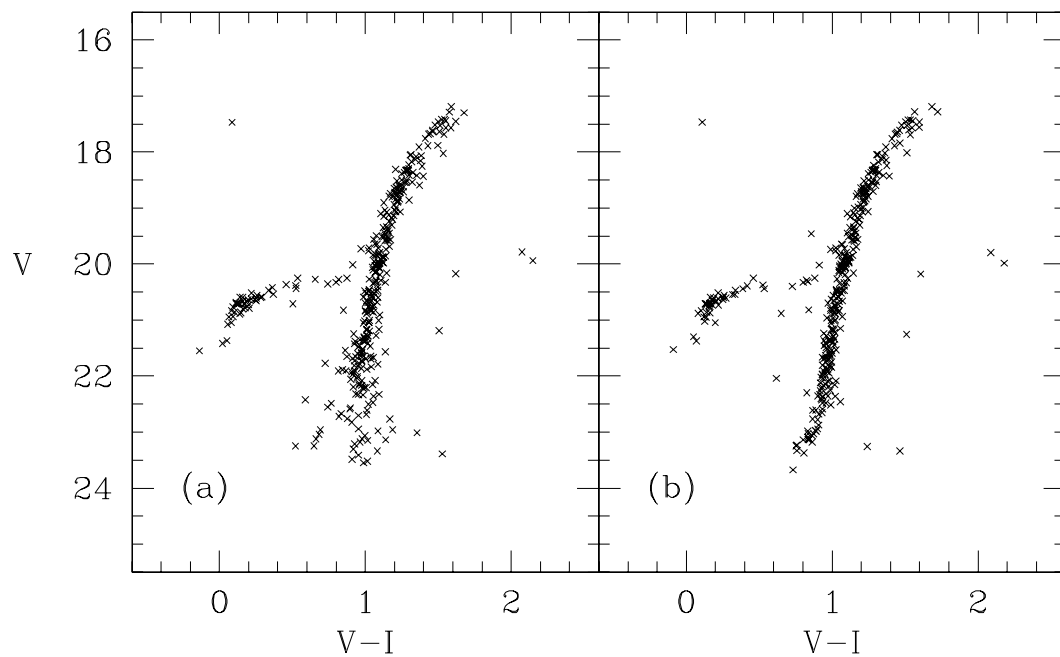
Stetson, CTE Effects in WFPC2 --- Fig. 1



Stetson, CTE Effects in WFPC2 --- Fig. 2



Stetson, CTE Effects in WFPC2 --- Fig. 3



Stetson, CTE Effects in WFPC2 --- Fig. 4